Korea-Australia Rheology Journal
Vol. 17, No. 4, December 2005 pp. 171-180

Numerical simulations of elliptic particle suspensions in sliding bi-periodic frames

Hee Taeg Chung, Shin Hyun Kang and Wook Ryol Hwang*
School of Mechanical and Aerospace Engineering, Engineering Research Institute, Gyeongsang National University, Gajwa-dong 900, Jinju 660-701, Korea.
(Received October 17, 2005; final revision received November 27, 2005)

Abstract

We present numerical results for inertialess elliptic particle suspensions in a Newtonian fluid subject to simple shear flow, using the sliding bi-periodic frame concept of Hwang *et al.* (2004) such that a particulate system with a small number of particles could represent a suspension system containing a large number of particles. We report the motion and configurational change of elliptic particles in simple shear flow and discuss the inter-relationship with the bulk shear stress behaviors through several example problems of a single, two-interacting and ten particle problems in a sliding bi-periodic frame. The main objective is to check the feasibility of the direct simulation method for understanding the relationship between the microstructural evolution and the bulk material behaviors.

Keywords : direct numerical simulation, elliptic particle suspension, sliding bi-periodic frame, bulk stress, elliptic integral of the second kind

1. Introduction

The system that a large number of elongated particles are suspended in a flow occurs in many industrial processes for the modification of mechanical, thermal or electrical behaviors of the material. A common example is the short fiber-filled thermoplastics that is widely used for an easy and efficient way for the reinforcement of polymeric products. Such a suspension is also important in pulp and paper industry.

When rods or fibers are suspended in a flow, the distribution of the particle orientation largely determines the flow properties of the composite material that is relevant to the final solid state material properties. Most of such suspensions are non-Brownian and the orientation of the individual particle is completely determined by the complicated hydrodynamic interaction not only from the neighboring particles but also from the ones far away. Therefore, especially in non-dilute suspensions, the direct numerical simulation technique that uses basic governing equations only is obviously promising in understanding the micro-scale evolution of the particle conguration and the orientational distribution and in predicting the bulk material properties. Yamane *et al.* (1994) developed a direct simulation method for the non-Brownian fiber suspension in simple shear flow where the short range interaction is modeled with the lubrication approximation, while the long range interaction being neglected. Fan *et al.* (1998) extended it in considering the long range interaction via the slender body approximation of Rahnama *et al.* (1995). However, with fast development of computational powers, another branch of direct numerical simulation techniques, without introducing the approximation modeling for the hydrodynamic interaction, has been widely used recently for particulate flow simulations. Among them, a special attention can be paid to the distributed Lagrangian multipliers (DLM) method by Glowinski *et al.* (1999) in that a fixed regular mesh can be used for the entire computation, including the interior of the particle, and that the hy-drodynamic interaction is treated implicitly by the combined weak formulation. Furthermore, one of the authors developed a direct numerical simulation techniques for particle suspensions by modifying the DLM method such that a small unit cell problem with a small number of particles can represent the system composed of a large number of particles by incorprating the Lees-Edwards type boundary conditions for the Molecular Dynamics to the continuous field problems of particle suspension flows (Lees and Edwards, 1972; Hwang *et al.*, 2004a).

The computational domain equipped with such a boundary condition is now called the sliding bi-periodic frame. They further showed that the method can be easily extended to the viscoelastic fluid medium and also to the three-dimensional spherical particle suspension formulated with both Newtonian fluid and a viscoelastic fluid, since it is based on the standard velocity-pressure formulation of the finite-element method (Hwang *et al.*, 2004b; 2004c).

*Corresponding author: wrhwang@gsnu.ac.kr
© 2005 by The Korean Society of Rheology

In this paper, we present numerical techniques and some preliminary results for non-Brownian elliptic particle suspensions in a Newtonian fluid subject to simple shear flow. Basically this work is an extension of Hwang *et al.* (2004a) by modifying the original method to deal with the elliptic particles. The main objective is to check the feasibility of the direct simulation method for the study of the inter-relationship between the microstructural changes in suspensions and the bulk material responses, without using the approximated interaction modelings. The paper is organized as follows: First, we state the governing sets of equations for the fluid, the particles and the hydrodynamic interaction in the strong form. Then we present the combined weak formulation for the whole system and discuss the implementation techniques, emphasizing the method for the uniform distribution of collocation points on the elliptic particle boundary. Subsequently, we present three sets of example problems the single, two and ten elliptic particles in a sliding bi-periodic frame to demonstrate the feasibility of our method and to discuss the relationship between the rheological properties and the microstructural evolution in elliptic particle suspensions.

2. Modeling

2.1. System

We consider freely suspended (i.e. force-free and torque-free) elliptic particles in a Newtonian fluid under 2-D simple shear flow, in which inertia is neglected for both fluid and particles. We employ the sliding bi-periodic frame of Hwang *et al.* (2004a) for the computational domain, in order to solve a large number of particle systems at a reasonable computational cost. Fig. 1 shows the sliding bi-periodic frames with a possible elliptic particle conguration in a single frame. Under simple shear flow, each frame translates at its own average flow velocity inside the frame and thereby each row of the frames slides relatively to one another by the amount Δ, which is determined by the given shear rate $\dot{\gamma}$, the elapsed time t, and the height of the frame H:

$$\Delta = \dot{\gamma} H t \tag{1}$$

The sliding velocity of the frame is determined by the given shear rate and a representative vertical position of the frame based on an arbitrary global reference. The frame is bi-periodic: the left and right boundaries satisfy the usual periodic condition and the upper and lower boundaries are subject to the time-dependent sliding periodicity described by Eq. (1). Therefore the motion of the particle as well as of the fluid is subject to the time-dependent coupling between the upper and lower boundaries, in addition to the usual periodic condition in the horizontal direction. For details of the sliding bi-periodic frame, refer to Hwang *et al.* (2004a).

A sliding bi-periodic frame, denoted by Ω, is the computational domain of the present work (Fig. 1). The four boundaries of the domain are denoted by Γ_i (i = 1, 2, 3, 4) and the symbol Γ will be used for $\cup_{i=1}^{4}\Gamma_i$. The Cartesian x and y coordinates are selected as parallel and normal to the shear flow direction, respectively. The regions occupied by the particle are denoted by P_i ($i = 1; ...; N$) and N is the number of particles in a single frame. We use a symbol $P(t)$ for $\cup_{i=1}^{N} P_i(t)$, a collective region occupied by the particles at a certain time t. For a particle P_i, $\boldsymbol{X}_i = (X_i, Y_i)$, $\boldsymbol{U}_i = (U_i, V_i)$, $\boldsymbol{\omega}_i = \omega_i \boldsymbol{k}$ and $\boldsymbol{\Theta}_i = \Theta_i \boldsymbol{k}$ are used for the coordinates of the particle center, the translational velocity, the angular velocity and the angular rotation, respectively; and $\boldsymbol{k}$ is the unit vector in the direction normal to the plane. The angular rotation of the particle Θ_i is measured from the positive y axis in the clockwise direction to directly compare with the Jeffery's solution (Larson, 1999).

2.2. Governing equations

The set of equations for the fluid domain is given by:

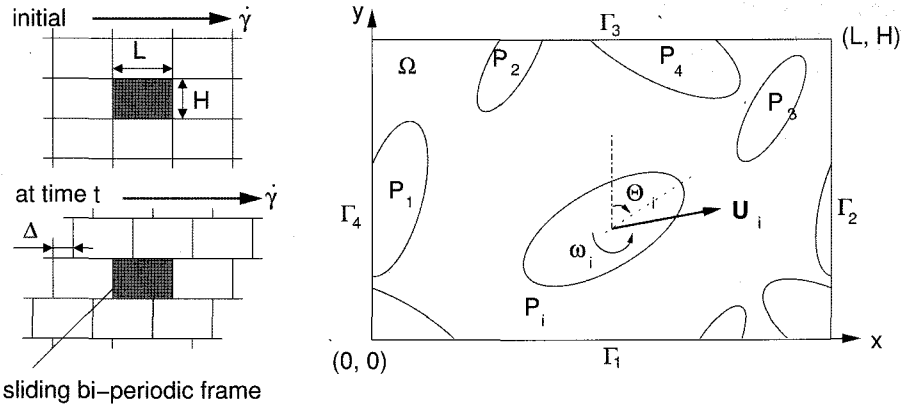

Fig. 1. The sliding bi-periodic frames in a simple shear flow (left). A sliding bi-periodic frame is the computational domain and a possible elliptic particle configuration inside the domain is illustrated (right).

$$\nabla \cdot \boldsymbol{\sigma} = 0, \quad \text{in } \Omega \setminus P(t), \tag{2}$$

$$\nabla \cdot \boldsymbol{u} = 0, \quad \text{in } \Omega \setminus P(t), \tag{3}$$

$$\boldsymbol{\sigma} = -p\boldsymbol{I} + 2\eta\boldsymbol{D}, \text{ in } \Omega \setminus P(t), \tag{4}$$

$$\boldsymbol{u} = \boldsymbol{U}_i + \boldsymbol{\omega}_i \times (\boldsymbol{x} - \boldsymbol{X}_i), \text{ on } \partial P_i(t), \ (i = 1, ..., N). \tag{5}$$

Eqs. (2-5) are equations for the momentum balance, the continuity, the constitutive relation, and rigid-body conditions on particle boundaries, respectively. Quantities u, σ, p, $\boldsymbol{I}$, $\boldsymbol{D}$ and η denote the velocity, the stress, the pressure, the identity tensor, the rate of deformation tensor and the viscosity, respectively. Unknown rigid-body motions in Eq. (5) will be determined by the hydrodynamic interaction. In the absence of the inertia, initial conditions are not necessary for the fluid velocity as well as for the particle.

On the domain boundary Γ subject to the sliding bi-periodicity, two conditions need to be satisfied: the continuity of the velocity field and the force (traction) balance. For the horizontal periodicity between Γ_2 and Γ_4, they can be written as

$$\boldsymbol{u}(0, y) = \boldsymbol{u}(L, y), \ y \in [0, H], \tag{6}$$

$$\boldsymbol{t}(0, y) = -\boldsymbol{t}(L, y), \ y \in [0, H], \tag{7}$$

where the vector $\boldsymbol{t}$ denoting the traction force on the boundary. The conditions for the vertical sliding periodicity between Γ_1 and Γ_3 are time-dependent and can be expressed as

$$\boldsymbol{u}(x, H; t) = \boldsymbol{u}(\{x - \dot{\gamma}Ht\}^*, 0; t) + \boldsymbol{f}, \ x \in [0, L), \tag{8}$$

$$\boldsymbol{t}(x, H; t) = -\boldsymbol{t}(\{x - \dot{\gamma}Ht\}^*, 0; t), \ x \in [0, L), \tag{9}$$

where $\boldsymbol{f} = (\dot{\gamma}H, 0)$ and $\{\cdot\}^*$ denotes the modular function of L: e.g., $\{1.7L\}^* = 0.7L$ and $\{-1.7L\} = 0.3L$.

Following the work by Hwang *et al.* (2004a, 2004b), we consider the elliptic particle as an elliptic rigid ring, which is filled with the same fluid as in the fluid domain and the rigid body condition is imposed on the particle boundary only. The idea is similar to the original immersed boundary method of Peskin (1972) in which the equations for the fluid velocity are solved for both inside and outside of the moving boundary of zero mass. The rigid-ring description needs a discretization only along the particle boundaries and leads to a significant reduction in memory usage. From the rigid-ring description, the set of governing equations for the region occupied by the particle becomes exactly the same as that of the fluid domain (Eqs. 2-5). The solution of the rigid-ring problem inside a particle is simply the rigid-body motion applied on the particle boundary, which is extended to the full particle interior:

$$\boldsymbol{u} = \boldsymbol{U}_i + \boldsymbol{\omega}_i \times (\boldsymbol{x} - \boldsymbol{X}_i) \text{ in } P_i(t). \tag{10}$$

In addition, the movement of the particle is given by the kinematic equations:

$$\frac{d\boldsymbol{X}_i}{dt} = \boldsymbol{U}_i, \quad \boldsymbol{X}_i|_{t=0} = \boldsymbol{X}_{i,0}, \tag{11}$$

$$\frac{d\Theta_i}{dt} = -\omega_i, \quad \Theta_i|_{t=0} = \Theta_{i,0}. \tag{12}$$

The minus sign in Eq. (12) is given due to the difference of the measuring direction between Θ and ω.

To determine the unknown rigid body motions ($\boldsymbol{U}_i$, ω_i)'s of the particles, one needs balance equations for the drag force and the torque on the particle boundaries. In the absence of inertia and external forces or torques, particles are force-free and torque-free:

$$\boldsymbol{F}_i = \int_{\partial P_i(t)} \boldsymbol{\sigma} \cdot \boldsymbol{n} \, ds = 0, \tag{13}$$

$$\boldsymbol{T}_i = \int_{\partial P_i(t)} (\boldsymbol{x} - \boldsymbol{X}_i) \times (\boldsymbol{\sigma} \cdot \boldsymbol{n}) \, ds = 0, \tag{14}$$

where $\boldsymbol{T}_i = T_i\boldsymbol{k}$ and $\boldsymbol{n}$ is a normal vector on ∂P_i pointing out of the particle ($i = 1, ..., N$).

We did not use an artificial particle-particle collision scheme (e.g. Glowinski *et al.*, 1999), because the particle overlap could be avoided for the multiple-particle problems we studied in this paper by taking a relatively small time-step and a sufficiently refined particle boundary discretization (Hwang *et al.*, 2004a; 2004b).

3. Numerical methods

Following the combined weak formulation of Glowinski *et al.* (1999) in which the hydrodynamic force and torque acting on the particle boundary cancel exactly, Hwang *et al.* (2004a) derived a weak form with the rigid-ring description of the particle in the sliding bi-periodic computation domain. We employ the same weak form in the present study that can be stated as follows:

Find $\boldsymbol{u} \in H^1(\Omega)^2$, $\boldsymbol{U}_i \in \Re^2$, $\omega_i \in \Re$, $\boldsymbol{\lambda}^{p,i} \in L^2(\partial P_i(t))$, $p \in L^2(\Omega)$, $\boldsymbol{\lambda}^h \in L^2(\Gamma_4)$, and $\boldsymbol{\lambda}^v \in L^2(\Gamma_3)$ ($i = 1, ..., N$) such that

$$\begin{aligned} &-\int_\Omega p \nabla \cdot \boldsymbol{v} dA + \int_\Omega 2\eta \boldsymbol{D}(\boldsymbol{u}) : \boldsymbol{D}(\boldsymbol{v}) dA \\ &+ \sum_i^N \langle \boldsymbol{\lambda}^{p,i}, \boldsymbol{v} - (\boldsymbol{V}_i + \boldsymbol{\chi}_i \times (\boldsymbol{x} - \boldsymbol{X}_i)) \rangle_{\partial P_i} \\ &+ \langle \boldsymbol{\lambda}^v, \boldsymbol{v}(x, H; t) - \boldsymbol{v}(\{x - \dot{\gamma}Ht\}^*, 0; t) \rangle_{\Gamma_3} \\ &+ \langle \boldsymbol{\lambda}^h, \boldsymbol{v}(0, y) - \boldsymbol{v}(L, y) \rangle_{\Gamma_4} = 0, \end{aligned} \tag{15}$$

$$\int_\Omega q \nabla \cdot \boldsymbol{u} dA = 0, \tag{16}$$

$$\langle \boldsymbol{\mu}^{p,i}, \boldsymbol{u} - (\boldsymbol{U}_i + \boldsymbol{\omega}_i \times (\boldsymbol{x} - \boldsymbol{X}_i)) \rangle_{\partial P_i} = 0, \ (i = 1, ..., N), \tag{17}$$

$$\langle \boldsymbol{\mu}^h, \boldsymbol{u}(0, y) - \boldsymbol{u}(L, y) \rangle_{\Gamma_4} = 0, \tag{18}$$

$$\langle \mu^v, u(x,H;t)-u(\{x-\dot{\gamma}Ht\}^*,0;t)\rangle_{\Gamma_3}=\langle \mu^v, f\rangle_{\Gamma_3}, \quad (19)$$

for all $v \in H^1(\Omega)^2$, $V_i \in \Re^2$, $\chi_i \in \Re$, $q \in L^2(\Omega)$, $\mu^{p,i} \in L^2(\partial P_i(t))$, $\mu^h \in L^2(\Gamma_4)$, and $\mu^v \in L^2(\Gamma_3)$ $(i=1, ..., N)$.

In the above formulation, three Lagrangian multipliers χ^p, λ^h and λ^v are introduced to combine the rigid body condition on the particle boundary (Eq. 5), the horizontal periodicity (Eq. 6) and the vertical sliding periodicity (Eq. 8), respective, as the constraints. The inner product $\langle \cdot, \cdot \rangle_s$ is the standard inner product in L^2 on s: $\langle \mu, v\rangle_s = \int \mu \cdot v \, ds$. We remark that the weak form needs to be modified when the particle crosses the boundaries of the computation domain. The modification has been treated in detail in Hwang *et al.* (2004a).

For the discretization of the weak form, we use regular quadrilateral elements with continuous bi-quadratic interpolation (Q_2) for the velocity u, and discontinuous linear interpolation (P_1) for the pressure p. The boundary integrals Eqs. (15) and (18) for the horizontal periodicity have been discretized by using the point collocation method for all nodes (nodal collocation), since the facing elements between Γ_2 and Γ_4 are conforming. For the vertical sliding periodicity between non-conforming elements on Γ_1 and Γ_3, we use the mortar element technique with the continuous linear interpolation of λ^v which has been verified to guarantee the optimal convergence of the kinematic compatibility and the force balance. Details on the sliding boundary integral can be found in Hwang *et al.* (2004a).

From the rigid-ring description, the discretization is necessary only along the particle boundary. In this study, the weak form of the rigid-ring description (Eq. 17) has been approximated by the point collocation:

$$\langle \mu^{p,i}(x), u(x)-(U_i+\omega_i \times (x-X_i))\rangle_{\partial P_i} \approx \sum_{k=1}^{M^i} \mu_k^{p,i} \cdot \{u(x_k)-(U_i+\omega_i \times (x-X_i))\}, \quad (20)$$

where M^i, x_k, and $\mu_k^{p,i}$ are the number of collocation points on ∂P_i, and the coordinate of the k-th collocation point on ∂P_i, and the collocated multiplier $\mu^{p,i}$ at x_k, respectively. An obvious reason for a choice of the point collocation is its simplicity in implementation especially for boundary-crossing particles. The implementation of Eq. (20) for the boundary crossing particle circumvents tedious boundary integrals over the splited particle boundary.

In order to guarantee the accuracy of the boundary integral in Eq. (20), one needs to distribute the collocation points on the particle boundary as uniformly as possible. Also care should be exercised in determining the number of the collocation points. An excessively large number of collocation points causes element-locking, while too small number of points is not capable to represent the rigid-body motion of the particle accurately. Unlikely to the circular particle case, obtaining the uniform distribution of points on the elliptic particle boundary is not obvious. The uniformity of points considered here means the equi-distance distribution of points with respect to the arclength. Consider an ellipse whose major axis b is parallel to y direction as in Fig. 2. The arclength s_i from θ_i to θ_{i+1} can be represented as

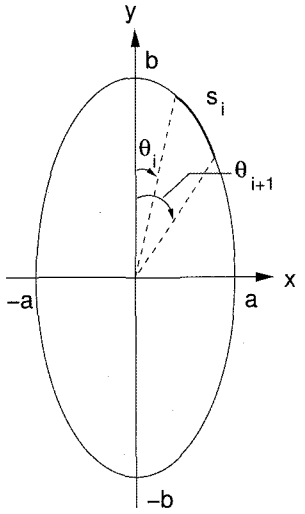

Fig. 2. The arclength s_i along the boundary of an ellipse can be evaluated by the elliptic integral of the second kind.

$$s_i = \int_{\theta_i}^{\theta_{i+1}} ds = b[E_I(\theta_{i+1},k)-E_I(\theta_i,k)], \quad (21)$$

where $k=\sqrt{1-a^2/b^2}$ and the integral $E_I(\theta, k)$ is called the elliptic integral of the second kind (Hildebrand 1976):

$$E_I(\theta,k) = \int_0^{\theta} \sqrt{1-k^2\sin^2\theta} d\theta \quad (22)$$

The perimeter P of an ellipse is evaluated as $4bE_I(\pi/2, k)$. In order to obtain the M evenly distributed points on the elliptic particle boundary, the arclength between the adjacent points needs to be P/M. This means that, for a given θ_i, the next collocation point θ_{i+1} is determined by the solution of the equation:

$$b[E_I(\theta_{i+1},k)-E_I(\theta_i,k)] = \frac{P}{M}. \quad (23)$$

In the present study, the above nonlinear equation has been solved by a simple incremental searching algorithm, considering that $\theta_{i+1} > \theta_i$. The number of the collocation points M for an ellipse has been determined by scaling the optimal number of collocation points for the circular particle of the same perimeter, which has been obtained in Hwang *et al.* (2004a). Approximately one collocation point per element appeared to be optimal in their work. See Fig. 3 for an illustrative example for discretizations for fluid and elliptic particles.

A set of equations with a sparse symmetric matrix with many zeroes on the diagonal appears as the result of the

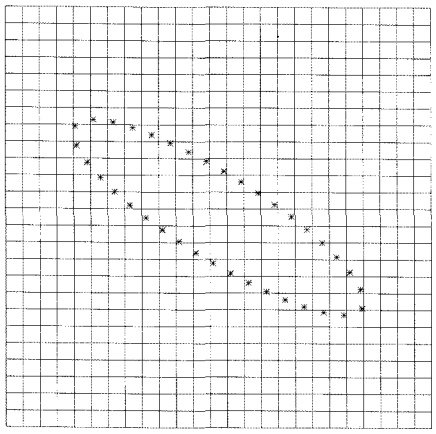

Fig. 3. The regular rectangular discretization is used for the entire computational domain and the particle is described by collocation points along the particle boundary.

above discretization, which has been solved by a direct method based on the sparse multi-frontal variant of the Gaussian elimination (HSL2002/MA41) for each time step. Once the rigid-body velocity of the particle is obtained as a part of the solution, the particle position and orientation for the next time step is calculated by integrating the kinematic equations (Eqs. 11 and 12) with the second-order Adams-Bashforth method.

Finally, we remark that the bulk stress, the average stress over the domain, in particle suspensions can be conveniently expressed by the boundary integrals over the domain boundary and the particle boundary, in terms of the Lagrangian multipliers λ^p, λ^h and λ^v (equivalent to the surface traction) in the sliding bi-periodic frame. The detailed mathematical derivation and the physical interpretation are in order in Hwang *et al.* (2004a). We use exactly the same expression to evaluate the bulk stress in the present study. For example, the bulk shear stress is evaluated by

$$\langle \sigma_{12} \rangle = -\frac{1}{L}\int_0^L \lambda_x^v(x)dx \tag{24}$$

4. Results

In this section, we present numerical results from the three sets of example problems: a single particle, two interacting particles, and ten particles in a sliding bi-periodic frame. Because of the sliding bi-periodicity of the computational domain, systems with a small number of particles in a single frame can represent a large number of such systems, eliminating unwanted wall effects.

To make comparison with the well-known analytical result of Jeffery, it would be better to briey review his work before presenting our simulation results. In 1922, Jeffery studied the motion of a single rigid neutrally-buoyant spheroidal particle in a linear Stokes flow (Larson, 1999). He showed that the angular rotation of the particle Θ in simple shear flow with the shear rate $\dot{\gamma}$, with the particle major axis in the plane of the deformation, can be expressed in time as:

$$\tan\Theta = a_s \tan\left(\frac{\dot{\gamma}a_s t}{a_s^2+1}\right), \tag{25}$$

where a_s is the particle aspect ratio and Θ is the angle of the axis of symmetry measured in the clockwise direction from the gradient direction of the flow. Eq. (25) indicates that the particle rotation is time-periodic and that the angular velocity of the particle is not uniform. The angular velocity becomes largest when the particle's major axis is in the gradient direction ($\Theta = 0$) and drops to a minimum when it aligned parallel to the flow direction ($\Theta = \pi/2$). This rotation is called the Jeffery orbit. The period of a complete rotation for the Jeffery orbit is

$$T = \frac{2\pi}{\dot{\gamma}}\left(a_s + \frac{1}{a_s}\right), \tag{26}$$

which is approximately $T \approx 2\pi a_s/\dot{\gamma}$ for a thin long spheroid ($a_s >> 1$).

4.1. A single elliptic particle in a sliding bi-periodic frame

The first example problem is a single elliptic particle at the center of the sliding bi-periodic frame of size 1×1 under the shear rate $\dot{\gamma} = 1$ with the fluid viscosity $\eta = 1$. We use several aspect ratio combinations with the major axis b and the minor axis a, keeping the same solid fraction ϕ to be 7.068%. (The area corresponds to the area of the circle with the radius $r = 0.15$). As depicted in Fig. 4, the single particle problem represents a large number regular configuration particles. There are two different time periods associated in this problem: the period of the sliding frame T_f and the period of the particle rotation T_p. The former T_f is determined by $L/\dot{\gamma}H$ (equal to one in this study), while the period of the particle rotation T_p is largely determined by the aspect ratio a_s, as implied in the Jeffery solution (Eq. 26). In general these two periods are not commensurate and this means that the single elliptic particle system is not time-periodic, which is distinct difference with the single circular particle problem in the sliding frame or with an isolated single particle problem.

Plotted in Fig. 5 is the particle angular velocity for three particle aspect ratios 1, 1.96 and 4. For the circular particle ($a_s = 1$), the angular velocity is around 0.5. The small fluctuation of the data originates from the period of the sliding frame T_f. For the elliptic particles, the absolute value of the angular velocity goes to the maximum when the major axis aligned normal to the flow direction and it reaches the minimum when the particle aligned in the flow direction, as illustrated in Fig. 5 (for $a_s = 4$). The evolution of the particle orientation is presented in Fig. 6, along with the com-

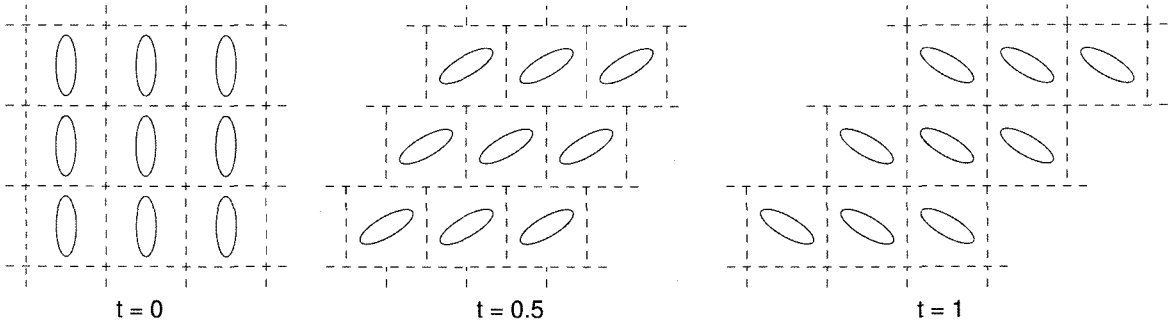

Fig. 4. The single particle problem in a sliding bi-periodic frame represents regular configuration of a large number of such systems. The period T_f of the frame configuration is $L/\dot{\gamma}H$ ('1' in this work).

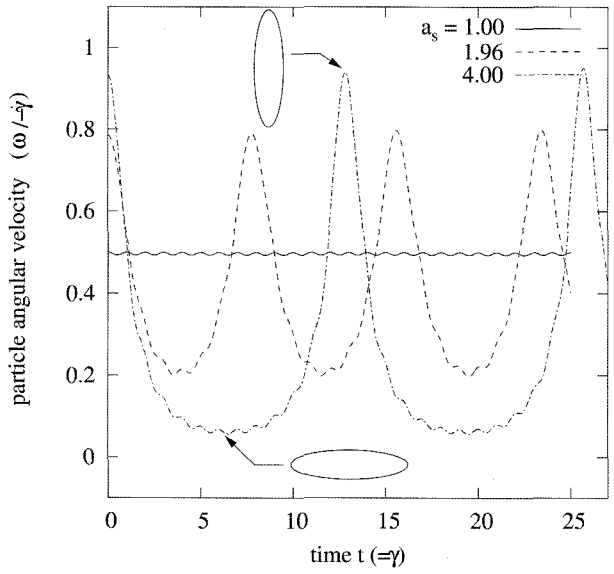

Fig. 5. The angular velocity of an elliptic particles in a sliding bi-periodic frame of 1 × 1 with $\dot{\gamma} = 1$ for three different particle aspect ratios $a_s = 1$, 1.96 and 4.

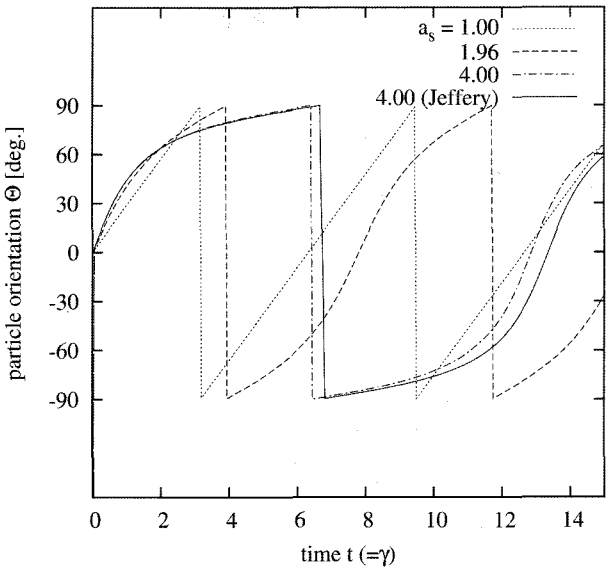

Fig. 6. The particle orientation Θ from the single particle problem for three different particle aspect ratios $a_s = 1$, 1.96 and 4. The straight line indicates the result from the Jeffery solution (Eq. 25) in case of $a_s = 4$ for comparison.

parison of the Jeffery solution (Eq. 25) for the particle with $a_s = 4$. The rotation of the elliptic particle is found to be similar to the Jeffery solution for the isolated spheroidal particle. The discrepancy with the Jeffery solution is caused not only by two-dimensionality of the problem, but also by the incommensurateness in the period of the single particle problem and the existence of other particles in the neighboring sliding frames. As plotted in Fig. 7, we also compared the period for a complete particle rotation for several particle aspect ratios with the Jeffery solution (Eq. 26). The result shows the similarity between the particle rotation of an elliptic particle with $\phi \approx 7\%$ in the sliding frame and an isolated spheroidal particle in simple shear flow.

In Fig. 8, we plotted the bulk shear stress in the single particle problem for the three cases. During one complete rotation of 360°, there are two local minimum and two local maximum orientation states in the elliptic single particle problem. The difference of the maximum and minimum stresses increases with the particle aspect ratio. The bulk stress gets lowered, when the particle major axis is aligned parallel or normal to the flow direction and it reaches the highest value when the particle orientation Θ is around ±45°. We note again that the shear stress data is not periodic because of the incommensurateness of the two frequencies in the single elliptic particle problem and there are small oscillations due to other particles contained neighboring sliding frames. The time-averaged bulk shear stress for these three cases is found to be almost the same in this small solid fraction example, though not presented here.

4.2. Two interacting elliptic particles in a sliding bi-periodic frame

The two elliptic particle problem is constructed to under-

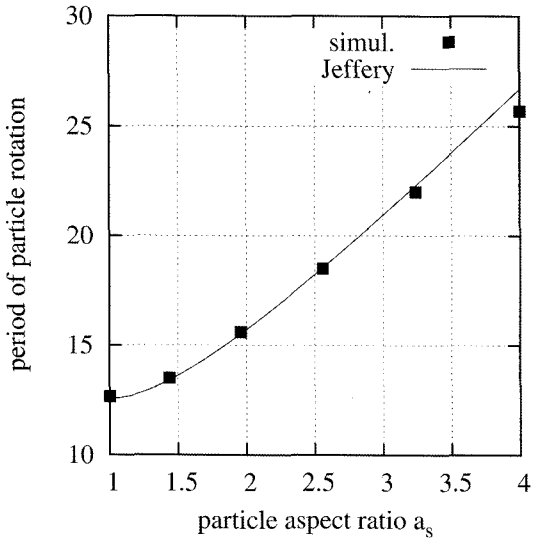

Fig. 7. The time required for a complete rotation of the elliptic particle in terms of the particle aspect ratio a_s. The straight line indicates the prediction from the Jeffery solution (Eq. 26).

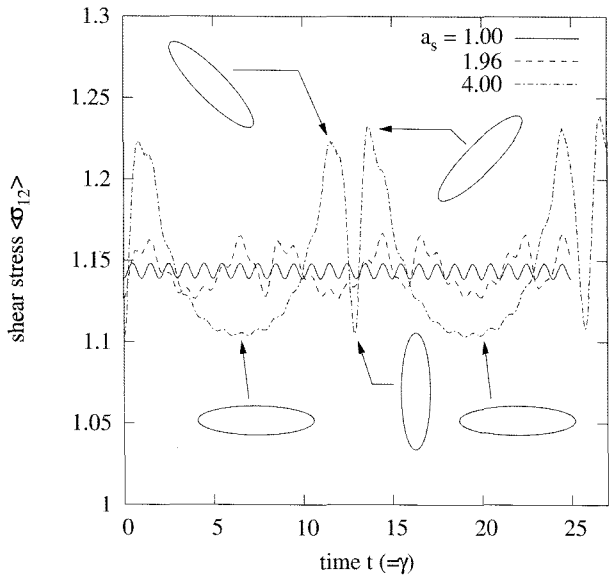

Fig. 8. The evolution of the bulk shear stress in time from the single particle problem for three different aspect ratios $a_s = 1$, 1.96 and 4. The particle orientation has been indicated for some of peak values (for $a_s = 4$).

stand how hydrodynamic interaction between two particles affects the orientation of the particles and the bulk stress. The initial particle configuration is shown in Fig. 9. The left particle, denoted by P_1, is oriented perpendicularly to the flow direction and the right particle P_2 is oriented obliquely with the rotation angle Θ_2. Initially, the same two particles are suspended freely at the position indicated in Fig. 9 under simple shear flow $\dot{\gamma} = 1$ with the fluid viscosity $\eta = 1$ in the sliding bi-periodic frame of the size

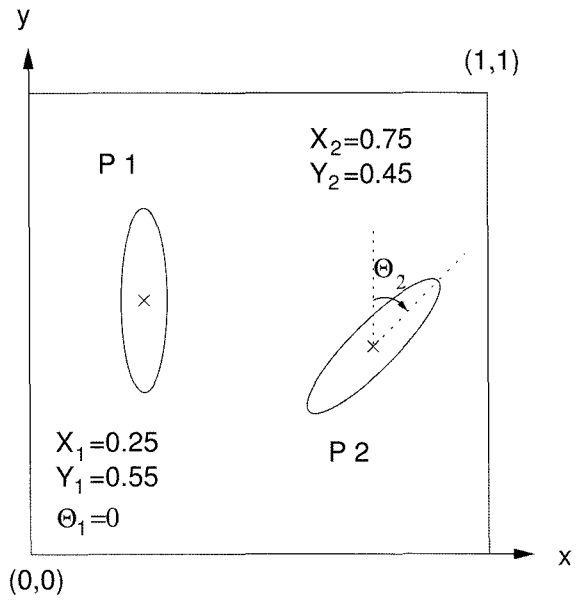

Fig. 9. The initial particle configuration of the two interacting particle problem.

1×1. The major and minor axes are 0.15 and 0.0375, respectively, and the aspect ratio a_s is 4 and the solid fraction $\phi = 3.53\%$. The zero velocity has been specified at the domain center (0.5, 0.5) such that P_1 is supposed to move to the right and P_2 translates towards the left. We performed numerical simulations for four different values of the initial orientation of P_2: $\Theta_2 = 0$, $\pi/4$, $\pi/2$, and $3\pi/4(=-\pi/4)$ (see Fig. 9).

The changes in the particle configuration in time for these four cases are presented in Fig. 10. At a glance, the two particles align in the flow direction when they approach closely each other (at $t = 5$) and this phenomenon is found to be independent of the initial particle orientation Θ_2. The rotation rate of the particle P_2 seems to be adjusted to result in the alignment when they approach closely. For example, the P_2 particle in case of $\Theta_2 = \pi/2$, which is already aligned in the flow direction initially, hardly rotates before the alignment with the other particle, while it rotates quickly in case of $\Theta_2 = 3\pi/4$. One can also observe that the particle configurations of $\Theta_2 = 0, \pi/4$ and $3\pi/4$ cases appear to be quite similar after the alignment occurs, although the initial orientation state of each problem is different. However, the P_2 in the $\Theta_2 = \pi/2$ case rotates relatively fast after the alignment.

The variations of the bulk shear stress in time for the four cases are plotted in Fig. 11. The comparison has been made with the result from the circular two particle problem with the same solid fraction at the same initial position as the elliptic particle problem. (In the circular particle case, the two particles kiss, tumble and separate symmetrically.) For all cases, two particles approach most closely around $t = 5$. From Fig. 11, one can observe that the bulk shear stress in

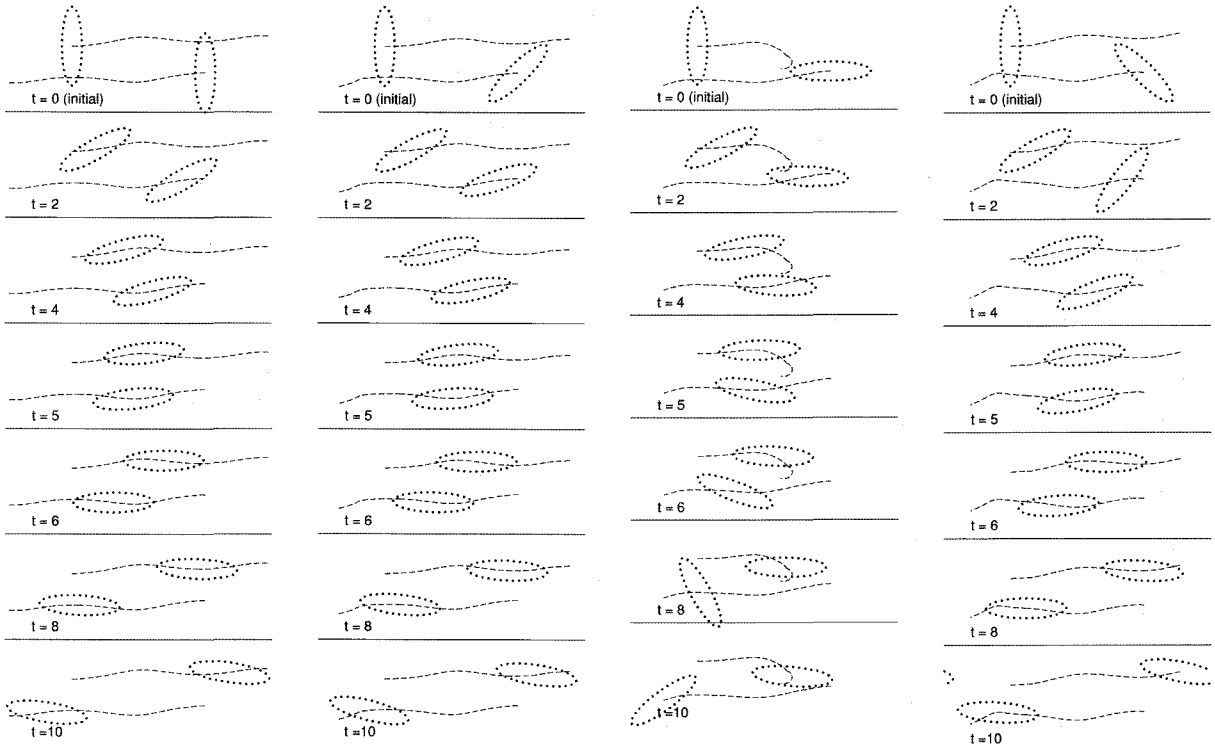

Fig. 10. The configurational change of the two interacting particles of four different initial particle orientation $\Theta_2 = 0$, $\pi/4$, $\pi/2$ and $3\pi/4$ (from left to right).

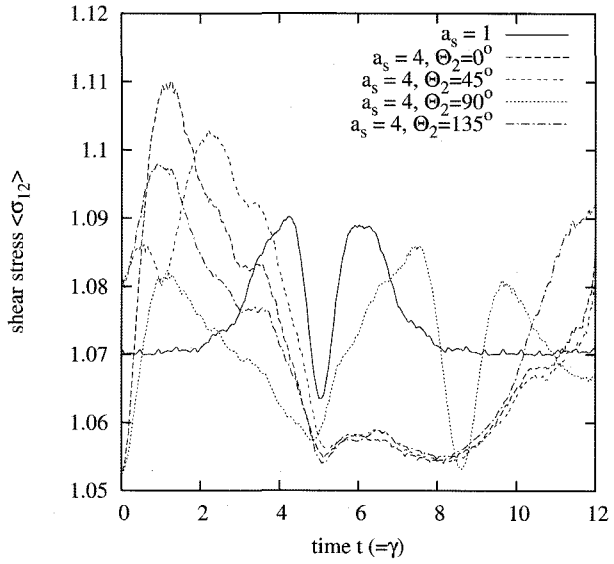

Fig. 11. The evolution of the bulk shear stress in time from the two interacting particle problems with $a_s = 4$ for four different initial particle orientation $\Theta_2 = 0$, $\pi/4$, $\pi/2$ and $3\pi/4$.

the elliptic particle problem is always lower than the circular particle case, when the two particles are aligned in the flow direction. The similar particle configuration after the alignment for $\Theta_2 = 0, \pi/4$ and $3\pi/4$ cases is also reflected in the bulk shear stress results for $t > 5$. Only the case with $\Theta_2 = \pi/2$ shows completely different shear stress behavior, as expected from Fig. 10.

4.3. Many particles in a sliding bi-periodic frame

The two previous problems are more or less restricted in investigation of the suspension behaviors because of the regularity in the particle configuration. In the last example, we attempt randomly distributed and oriented many elliptic particles in the sliding bi-periodic frame. The problem is stated as follows: randomly distributed and oriented the same ten elliptic particles of the aspect ratio $a_s = 4$, the major axis being 0.2 and the minor axis being 0.05, are suspended initially in the sliding bi-periodic frame of the size 1×1 under the shear rate $\dot{\gamma} = 1$ and the fluid viscosity $\eta = 1$. The solid fraction ϕ is 31.41%. The comparison has been made with the circular ten particle problem with the same solid fraction. The initial configurations of the two problems are indicated in Fig. 12.

Plotted in Fig. 13 are the evolution of the particle orientation of the elliptic particle problem. The result has been compared with the Jeffery solution for $a_s = 4$. Fig. 13 shows that particles aligned mostly in the flow direction after $t = 4$. Comparing the numerical result with the Jeffery solution, the elliptic particles in the concentrated suspension largely orient in the flow direction faster than in the dilute system of the Jeffery solution. The bulk shear stress

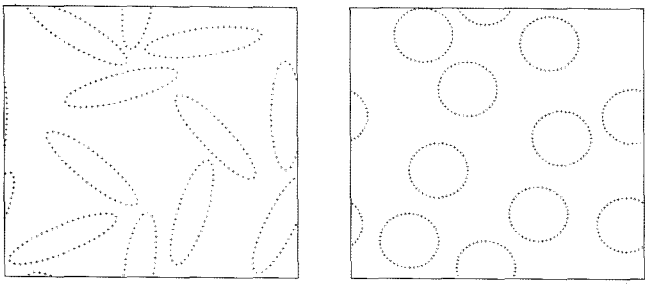

Fig. 12. The initial particle configuration of ten particle problems: elliptic particles of $a_s = 4$ (left); circular particles ($a_s = 1$) (right). Both the problems have the same solid area fraction $\phi = 31.41\%$.

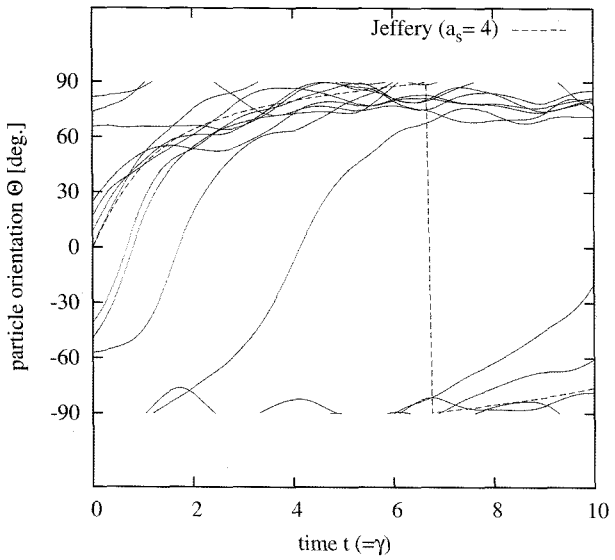

Fig. 13. The evolution of the orientation Θ of the ten elliptic particle problem. The dashed line indicates the Jeffery orbit of $a_s = 4$.

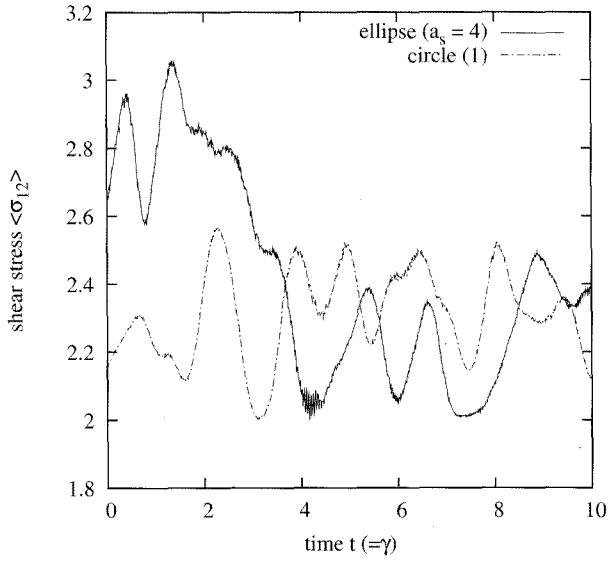

Fig. 14. The bulk shear stress of the ten particle problems in time.

results of the two problems are presented in Fig. 14. The fluctuation in the bulk stress data of the elliptic particle problem is found to be larger than in the circular particle problem due to the orientation effect. The shear stress gets lowered after $t = 4$ in case of the elliptic particle problem, at which the particles aligned in the flow direction as mentioned with Fig. 13. We plotted the instantaneous total shear rate (the second invariant of the rate-of-deformation tensor $2\boldsymbol{D}$) with the particle configuration at $t = 1.4$ and $t = 7.2$ in Fig. 15. The former corresponds to the instant when the bulk shear stress is the highest and the latter is the time when it is the lowest in Fig. 14. At $t = 1.4$, the distribution of the particle orientation is random and the shear rate (i.e. the stress) is found to be high in the vicinity of the particles. In contrast, the particles aligned almost parallel to the flow direction at $t = 7.2$ and the stress near the particle is relatively lowered compared with the result at $t = 1.4$.

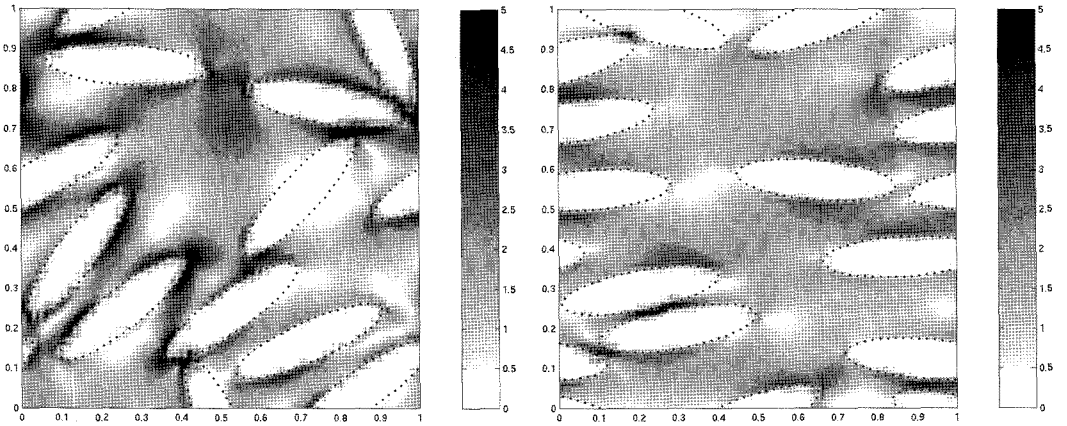

Fig. 15. The instant shear rate distribution when the bulk shear stress in Fig. 14 reaches the highest peak at $t = 1.4$ (left) and the stress goes to the lowest value at $t = 7.2$ (right).

This distinct stress distribution around the particle seems to be responsible for the bulk shear stress difference between these two states.

5. Conclusions

In this work, we presented a finite-element formulation and implementation techniques for direct numerical simflulations for elliptic particle suspensions in a Newtonian fluid subject to simple shear flow. We employed the sliding bi-periodic frame as the computational domain to deal with a large number of particle systems within reasonable computation cost. In the present method, it is not necessary to introduce approximation modelings for hydrodynamic interaction between particles.

The computational domain is discretized regularly with bi-quadratic interpolation of the velocity and linear discontinuous interpolation of the pressure. The sliding bi-periodic constraints are implemented by the mortar element method. The point collocation method has been used to assign rigidity of the particle via rigid-ring description on the particle boundary. To guarantee the numerical accuracy, we implemented the elliptic integral of the second kind numerically to distribute collocation point as uniformly as possible on the elliptic particle boundary. To demonstrate the feasibility of our method, we present three sets of example problems: the single, two interacting particles and ten particles in a sliding bi-periodic frame, which represent infinite number of such systems in the unbounded domain. In the single elliptic particle problem, we presented the particle rotation rate for several particle aspect ratios and discussed the particle orientation effect on the bulk shear stress (i.e. viscosity) of the system. From the two elliptic particle problem, we demonstrated the configurational change of particles when they interact each other in simple shear flow and presented the evolution of the bulk shear stress on these occasions. As a test problem for concentrated suspension with a large number of particle, we presented ten particle problems and showed the change of the particle orientation and the bulk shear stress, along with the comparison with the circular particle suspensions with the same solid fraction.

Acknowledgment

This work has been supported by Research Center for Aircraft Parts Technology (ReCAPT), Gyeongsang National University.

References

Fan, X., N. Phan-Thien and R. Zheng, 1998, A direct simulation of fibre suspensions, *J. Non-Newtonian Fluid Mech.* **74**, 113-135.

Glowinski, R., T.-W. Pan, T.I. Hesla and D.D. Joseph, 1999, A distributed Lagrangian multiplier/fictitious domain method for particulate flows. *Intern. J. Multiphase Flows* **25**, 755-749.

Hildebrand, F.B., 1976, Advanced Calculus for Applications, Prentice-Hall, New Jersey.

Hwang, W.R., M.A. Hulsen and H.E.H. Meijer, 2004a, Direct simulation of particle suspensions in sliding bi-periodic frames, *J. Comput. Phys.* **194**, 742-772.

Hwang, W.R., M.A. Hulsen and H.E.H. Meijer, 2004b, Direct simulations of particle suspensions in a viscoelastic fluid in sliding bi-periodic frames, *J. Non-Newtonian Fluid Mech.* **121**, 15-33.

Hwang, W.R., M.A. Hulsen, H.E.H. Meijer and T.H. Kwon, 2004c, Direct numerical simulations of suspensions of spherical particles in a viscoelastic fluid in sliding tri-periodic domains, in *Proceedings of the XIVth International Congress on Rheology*, Seoul, Korea, August 22-27, CR10.1-CR10.3.

Larson, R.G., 1999, The structure and rheology of complex fluids, Oxford University Press.

Lees, A.W. and S.F. Edwards, 1972, The computer study of transport processes under extreme conditions, *J. Phys. C: Solid State Phys.* **5**, 1921-1929.

Peskin, C.S., 1972, Flow patterns around heart valves: a numerical method, *J. Comput. Phys.* **10**, 252-271.

Rahnama, M., D.L. Koch and E.S.G. Shaqfeh, 1995, The effect of hydrodynamic interactions on the orientation distribution in a fiber suspension subject to simple shear flow, *Phys. Fluids A* **2**, 2093-2102.

Yamane, Y., Y. Kaneda and M. Doi, 1994, Numerical simulation of semi-dilute suspensions of rodlike particles in shear flow, *J. Non-Newtonian Fluid Mech.* **54**, 405-421.